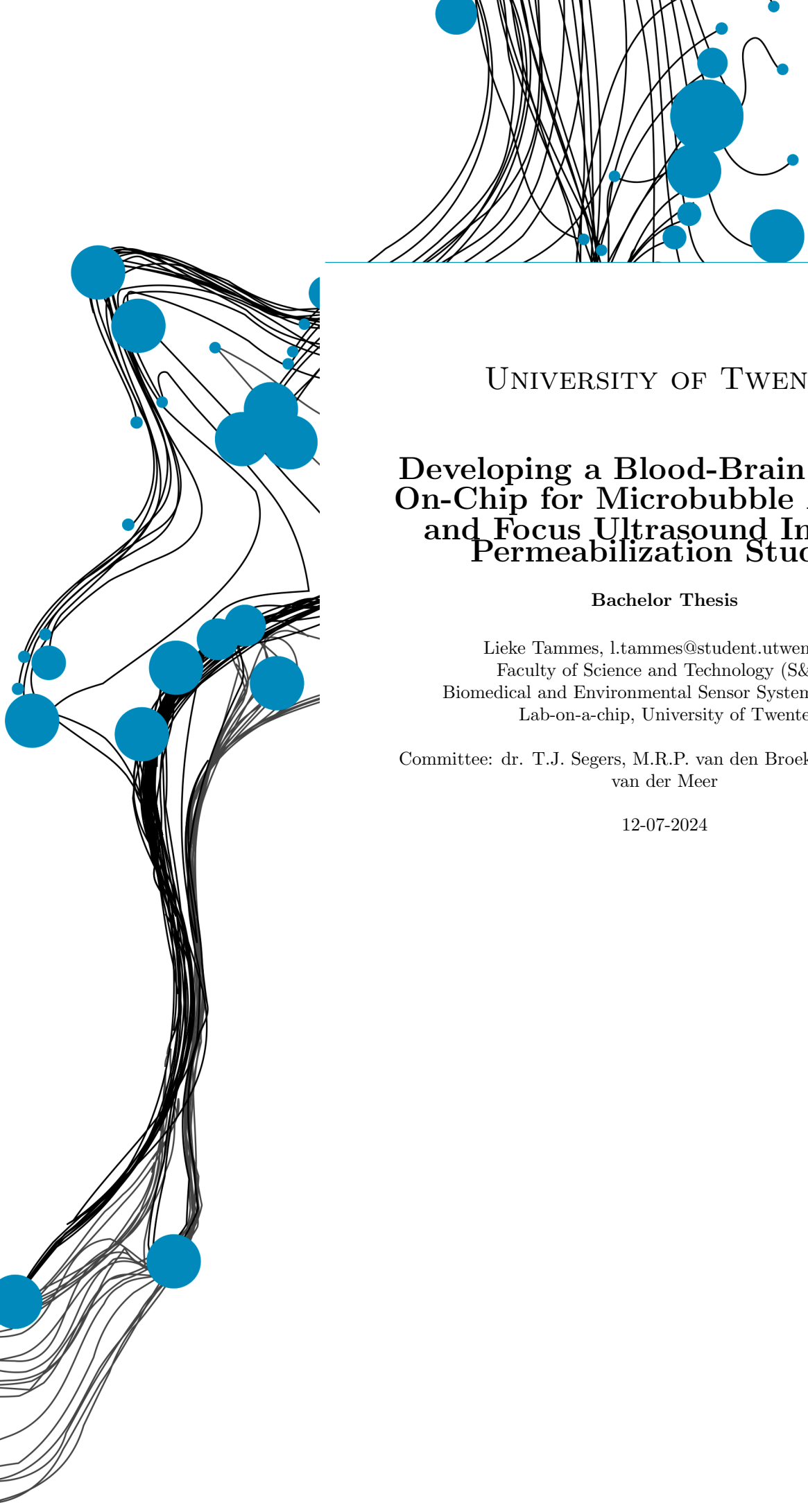

University of Twente

Developing a Blood-Brain Barrier On-Chip for Microbubble Assisted and Focus Ultrasound Induced Permeabilization Studies

Bachelor Thesis

Lieke Tammes, l.tammes@student.utwente.nl
Faculty of Science and Technology (S&T)
Biomedical and Environmental Sensor Systems (BIOS)
Lab-on-a-chip, University of Twente

Committee: dr. T.J. Segers, M.R.P. van den Broek, prof.dr. A.D. van der Meer

12-07-2024

Abstract

This study investigates the issues related to cell culture stability and monolayer formation in microfluidic chips for microbubble-assisted focused-ultrasound induced blood-brain barrier permeabilization. Current research is exploring microbubble-assisted focused-ultrasound to locally and non-invasively permeabilize the blood-brain barrier, using an in vitro blood-brain-barrier-on-chip model. To solve the reproducibility issues this model-on-chip has, this report has designed a new chip, meant to be used with applied flow. The new chip design will allow live cell imaging and for this purpose accommodate an objective lens between the pipette points for precise imaging. Calculations determined that the resulting shear stress on the cells was 1.98 $dyne/cm^2$, which is in the range of physiological shear stress. The chip fabrication process involved creating molds using micromilling, SU-8 clean room fabrication, and 3D-printing, with the SU-8 mold proving to be most suitable for making chip with the desired qualities. Chips were prepared by pouring a PDMS mixture over the mold, curing it, and bonding the membrane to the chip parts after oxygen plasma treatment. Cell culture experiments used induced pluripotent stem cells differentiated into endothelial cells, seeded into the chips and subsequently incubated, with flow applied to some chips to study its effects. The first two experiments had a low cell survival rate and the third experiment showed a diminishing of cell confluency over time. Analysis using microscopy and ImageJ revealed variability in cell monolayer confluence. It is suggested that this variability could be due to surface hydrophobicity or the delicate nature of induced pluripotent stem cells. It is recommended to repeat the research, focussing on only one aspect at a time.

1 Introduction

The blood-brain barrier (BBB) is one of the main components that protects the brain from chemical and pathogenic threats, by separating the blood, which could contain toxic foreign substances, from the brain's extracellular fluid [1]. The BBB consists of multiple different celtypes, a schematic of which can be found in Figure 1. The most important cell type are the brain microvascular endothelial cells (BMECs), which are situated in a tight monolayer and regulate transport of nutrients and waste. Its unique properties are due to their membrane proteins; tight junctions (TJs), such as occludin, claudins, and zonula occludens (ZO), and adherent junctions (AJ), such as cadherins, catenins, vinculin, and actinin. These junctions act as bridges between the cells, impeding them from moving away from each other. BMECs line the blood vessel walls which run through the brain [1, 2, 3]. On the brain side of the blood vessel multiple cell types influence BBB formation and maintenance, most importantly the astrocytes and pericytes. Pericytes play an important part in angiogenesis, the formation of new blood vessels. They also use paracrine signals to promote TJ formation and seal the BMEC layer. Astrocyte endfeet have a similar function, where they encircle the blood vessels and anchor them to the basal lamina, providing support to the blood vessel wall. Astrocytes also secrete factors which can promote or inhibit pathways relating to the transport of molecules through the BMECs. The communication between these cells and the BMECs is integral for the impermeability of the BBB [4, 5]. The BBB prevents almost all macromolecules and 95% of small molecules (<1kD) from penetrating through to the brain. This mechanism prevents viruses and other harmful substances from getting into the brain, however in the presence of conditions such as a tumor or a neurodegenerative disease, the mechanism also impedes medicine from reaching the brain for treatment [6, 7, 2].

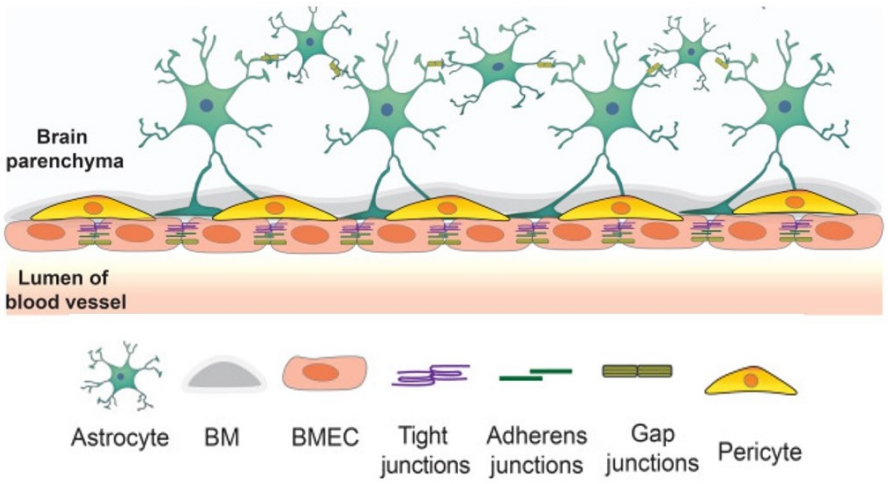

Figure 1: Schematic of the BBB. The BMECs are attached to each other, through cell junctions. Astrocyte endfeet and pericytes communicate with the BMECs to maintain the impermeability of the BBB [4].

Due to this low permeability of the BBB, current clinical treatment options for neurological disorders are either invasive or non-specific, or have a high toxicity [6, 2]. Such as for Alzheimer's Disease, where a lot of drugs don't make it out of the trial phase due to permeability issues at the BBB. The low permeability also results in higher dosages of the drugs, which increases the chance of undesired secondary effects [8]. For brain tumors, the preferred treatment is surgery, radiotherapy, immunotherapy and/or chemotherapy. Limitations of surgery are the long patient recovery time, high risk of infections and the possibility of loss of functionality due to the resection of brain tissue. Both radiotherapy and chemotherapy have a lot of undesired side effects, such as nausea and severe fatigue. Immunotherapy has similar side effects, although the specific effects may vary, additionally immunotherapy is effective only if the tumor has the appropriate receptors on its cellmembrane [6, 9]. A lot of patients are left with cognitive deficits after treatment for brain tumors, as all treatment options also impact the surrounding healthy brain tissue, either by being cut out for clean margins, or due to the non-specific effects [9].

Microbubble-assisted focused-ultrasound induced (MB+FUS) BBB permeabilization is a non-invasive method that is currently being researched to locally permeabilize the BBB [7, 10]. This method for BBB disruption (BBBD) depends on gas filled microbubbles (MBs) coated with either albumin or phospholipids. After injection these MBs are then exposed to ultrasound waves, which makes the MBs expand and contract at the frequency of the propagating acoustic wave. This is due to the wave propagation resulting in cyclic pressure reduction and increase. MB behaviour is dependent on the size of the MB and the ultrasound driving type, however there is considerable debate regarding the underlying mechanism [11]. In current research at the chair BIOS Lab-on-a-chip (University of Twente) [10], the mechanism with which MBs permeabilize the BBB is studied. They are researching under which conditions safe, controlled and reversible BBB permeabilization happens and which bubble gives the best result. For this an *in vitro* BBB on-chip model is used. This model consists of induced pluripotent stem cells (iPSC) derived BMECs inside a chip. The chips consist of a bottom layer, with a channel and a top layer with a channel, attached in between is a membrane to which cells are attached from the bottom channel, see Figure 2.

Figure 2: Cross-section view of a standard BBB-chip, with from top to bottom the top part including the top channel, the porous membrane, the iPSC monolayer, which is attached to the membrane and the bottom part including the bottom channel. The schematic is not to scale.

This iPSC-model on chip has a high level of variability and a low level of reproducibility, which has been recorded previously [3, 10]. The primary issue identified was the cells being washed out where the channels overlap, which resulted in holes in the monolayer.

In vivo the BBB experiences shear stress from blood flow, which provides the cells with information about it's surroundings and helps elicit an appropriate response, such as monolayer formation. Flow induced shear stress has been proven to enhance BBB performance by promoting tight junctions formation [12, 13, 14]. In vivo the shear stress is equal to about 5 $dyne/cm^2$ [15, 16], which corresponds to a flow rate of about $0.5-1.5$ mm/s in capillaries, small vessels with a diameter <10 µm [17, 18] and $1-10$ mm/s for vessels with a diameter of 20-70 µm [19]. Therefore, introducing shear stress to the chip model is expected to enhance tight junctions formation, which is expected to improve the resistance of the cells to being washed out. A different geometry could also enhance cell yield after culturing. In the previous model [10] a small overlap of 500 µm by 500 µm was used. By enlarging the overlap between the two channels, a higher percentage of the cells will be in the overlapping part of the channel.
This report will research the effect of the geometry and flow on the TJ-expression and monolayer formation of a BBB on-chip meant for MB+FUS permeabilization studies.

2 Chip Design

The chip, which is currently being used, had a design similar to Figure 3, with a channel height of 375 µm, a width of 500 µm, and a channel length of 1.3 cm. These will be referred to as the small chips, as the newly designed chips will be considerable bigger. Only recently have they started experimenting with the big overlap.

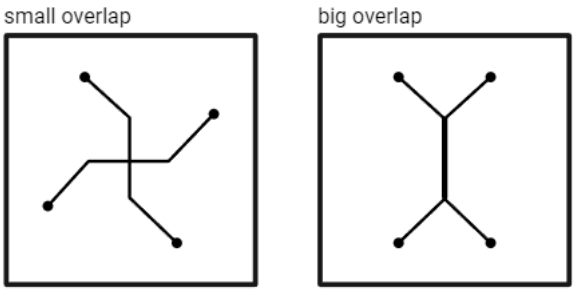

Figure 3: Top view of the small chips, with a channel height of 375 µm and a channel width of 500 µm.

The new chip will be designed for MB+FUS permeabilization studies. For these studies it is important that the MBs and the cells can be imaged with a microscope. To do this the chip needs to be transparent, this is why PDMS will be used to make the chip. The imaging should be able to be done while the cells are still alive, meaning that there will be pipette points with medium still in the chip to keep the cells alive. To fit an objective in between these pipette points, the distanced between the pipette points was measured to be 29 mm. To be able to image the cells, the objective has to be able to almost touch the chip, as most objectives have a working distance of only a few milimeters, which is very close to the heigth of the chip and definitely closer than the height of the pipette tips. It is not possible to put the chip upside down, due to the MB+FUS setup. Thus the objective needs to fit in between the pipette tips, which means that the bottom channel will have a length of 30 mm. The width of the channel was fixed to 500 µm, which is smaller than the ultrasound focal width, as resonance in the channel will result in MBs in different places having different behaviour, whereas uniform behaviour is desired.

$$\Delta P = \rho \cdot g \cdot H \tag{1}$$

In which, ΔP is the pressure difference in Pa due to the rocker, ρ is the density of the liquid inside the channel in kg/m^3, g is the gravity, which is a constant at 9.81 m/s^2 and H is the height the rocker provides where the horizon is 0° in m. The angle of the rocker was then determined using Formula 2.

$$sin(\theta) = \frac{H}{L} \tag{2}$$

In which θ is the angle in degrees of the rocker, H is the height in cm the rocker provides where the horizon is 0°, and L is the length of the channel in cm.
Using the equation for flow from the lectures of Henrik Bruus [20] and rewriting it for pressure:

$$\begin{aligned} Q &= [1 - 0,63(\frac{h}{w})] \cdot \frac{h^3 w \Delta P}{12\eta L} \\ \Delta P &= \frac{Q}{1 - 0,63(\frac{h}{w})} \cdot \frac{12\eta L}{h^3 w} \end{aligned} \tag{3}$$

In which Q is the flow in the channel in m^3/s, h is the channel height, w is the channel width, ΔP is the pressure difference in Pa, η is the viscosity in $Pa \cdot s$, and L is the length of the channel in m.
Using that:

$$Q = A \cdot v = h \cdot w \cdot v \tag{4}$$

$$\Delta P = \frac{1}{1-0,63(h/w)} \cdot \frac{12\mu L}{h^3 w} \cdot h \cdot v \cdot w$$

$$\Delta P = \frac{12\eta L \cdot h \cdot w \cdot v}{[1-0,63(h/w)] \cdot h^3 \cdot w} \tag{5}$$

$$\Delta P = \frac{12\eta L \cdot v}{[1-0,63(h/w)] \cdot h^2}$$

The channel length was determined to be $3cm = 0.03m$, the viscosity was set to $1 \cdot 10^{-}3\ Pa \cdot s$. This resulted in a final equation for the pressure difference:

$$\Delta P = \frac{0.00036v}{[1-0,63(h/w)] \cdot h^2} \tag{6}$$

To determine the shear stress on the cells, Equation 7 can be used.

$$\tau = \eta \frac{dv}{dy} \tag{7}$$

In which τ is the shear stress in Pa, and $\frac{dv}{dy}$ is the derivative of the veloctiy to the height in the channel. This can be simplified to be:

$$\begin{aligned} \tau &= \eta \frac{\Delta v}{\Delta y} \\ \tau &= \eta \frac{v_{max} - 0}{\frac{1}{2}h - 0} \\ \tau &= \eta \frac{2 \cdot v_{max}}{h} \\ \tau &= \eta \frac{2 \cdot 2V_{gem}}{h} \\ \tau &= \frac{\eta \cdot 4 \cdot v}{h} \end{aligned} \tag{8}$$

A matlab script was made using Equation 1, 2, 6 and the end result of Equation 8. The remaining variables could be filled in to get to an adequate velocity and shear stress through trial and error. The matlab script can be found in Appendix 5.
The values calculated with the matlab script can be found in Table 1. A shear stress of 5 $dyne/cm^2$ is in the range of physiological shear stress values. The final chip design, based on these calculations can be found in Figure 4.

Table 1: Values determined using the matlab script.

Physical quantitiy	Value	Unit
Rocker angle	46	$degrees$
Height	250	μm
Width	500	μm
Pressure	211.7	Pa
Velocity	25.2	mm/s
Shear stress	4.03	$dyne/cm^2$

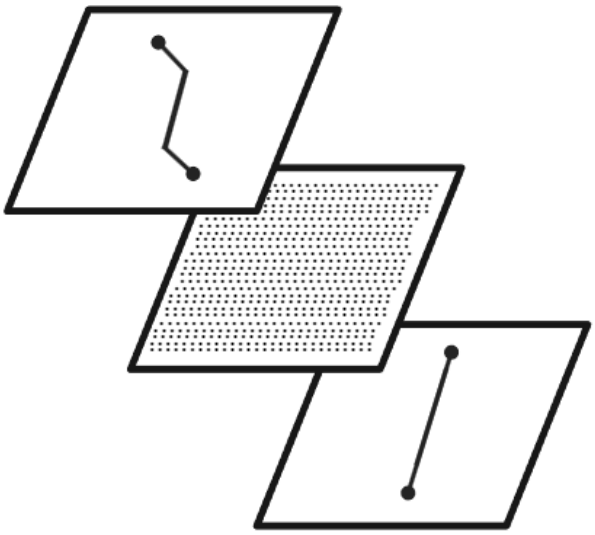

(a) The chip design, the top part can be rotated 90°, depending on the overlap size. In between the bottom and the top channel is a PDMS membrane of 2 µm thickness and 5 µm pores.

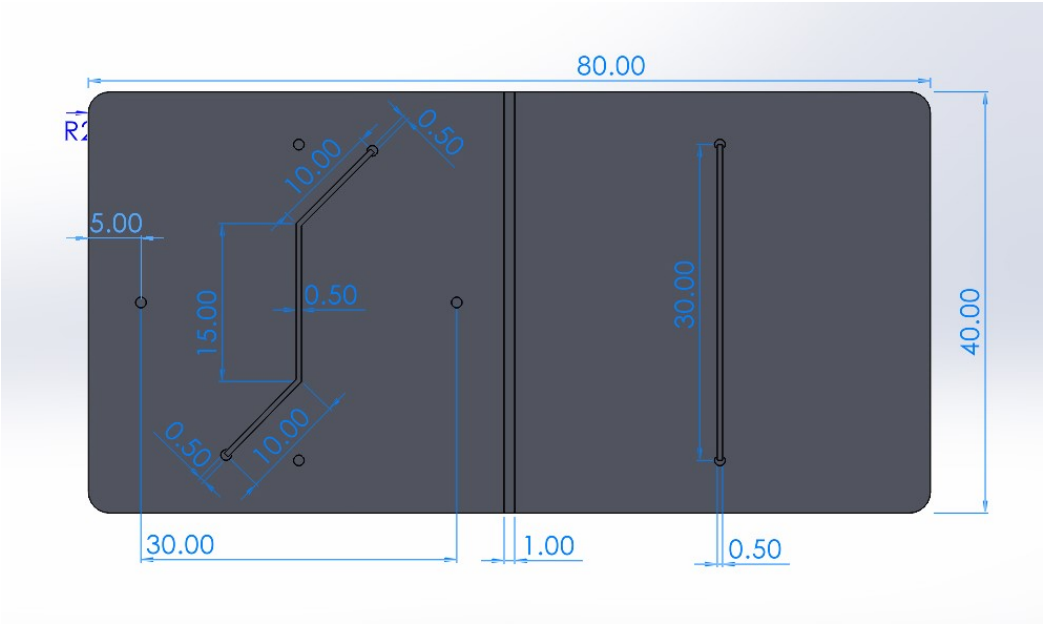

(b) The mold for the chip, designed in Solidworks, with dimensions shown in mm. The height of the channels is 0.25 mm.

Figure 4: Graphical view of the designed chip. The round holes are the inlets and can be punched open depending on what the orientation of the bottom part is.

For the small overlap the top and bottom part can be put together at a 90° degree angle. For the big overlap, the top and bottom part should be put together like in Figure 4.
The mold design was made three different ways; it was micromilled from PMMA, made using stereolithography with Grey Pro Resin (Grey Pro Resin (Form 3), formlabs) and a SU-8 mold was made in the clean room. The first two molds had a high surface roughness, which resulted in the chips not being transparent enough to culture cells inside. Aside from that, the mold made with stereolithography bent, making it harder for the top and bottom part to bond together. The SU-8 mold, was transparent, however when fabricating the mold, the channel height had to be adjusted to 200 µm.
Unfortunately, the previously calculated angle of 46° could not be reached with the rocker that was used. The maximum angle this rocker could reach was 24°. This resulted in a lower shear stress on the cells, which was recalculated using the matlab script, resulting in a new shear stress of 1.98 $dyne/cm^2$, which is still in range of the physiological shear stress and is therefore still relevant.

3 Cell Culture

3.1 Chip Fabrication

SolidWorks was used to make a model of the mold for the designed chip. This model was turned into a mold by micromilling, by clean room fabrication with SU-8 and 3D-printing. The SU-8 mold was used for chip making, as this mold had the desired qualities, see Figure 1.
A porous 2 µm thick PDMS membrane (pore diameter of 5 µm and a 30 µm pitch) was prepared using the protocol of Zacharova *et al.* [21].
To make the chip the protocol of Van der Helm *et al.* [22] was used. In short, a 10:1 PDMS:curing agent mixture was poured over the mold and, after degassing in vacuum to get rid of airbubbles in the chip, as the airbubbles could impact the visibility of the cells in the chip, put in the oven at 60°C to cure. Once cured, the chips were cut and 1 mm inlets were punched in the top part.
The membrane was cut into pieces that would cover the full overlap with a diamond pen. The top part of the chip and the membrane were bonded after oxygen plasma treatment in the plasma oven (CUTE, Femto Science, Besançon, France). After strengthening the bonding by leaving the chip with membrane in the oven for 10-15 minutes, the wafer was detached using acetone to dissolve the photo-resist. Subsequently the membranes were checked for defects by microscopy. After leaving the top part to evaporate in the fume hood for 60 minutes, the bottom part and top part were bonded, making sure to align the channels, leaving it in the oven at 60°C to strengthen the bonding for 10-15 minutes after.
Before seeding, the chips were oxygen plasma treated, to create hydrophilic channels. Subsequently, the chips were transferred to the laminar flow cabinet and were flushed with ethanol 70%, to clean them of impurities which could impact the microfluidic resistance, and thrice with PBS, to make sure all the ethanol was out of the chip as this could cause the cells to die. The chips were flushed with Collagen type I rat tail (Corning Inc., New York, USA and, Gibco, Thermo Fischer Scientific, Massachusetts, USA) at a concentration of 100 µg/mL in PBS and left for about 60 minutes at 37°C. Afterwards the chips were flushed with phosphate buffered saline (PBS).

3.2 Cell Culture

The cell culture was performed three times to quantify reproducibility. Different compositions of chips were used per experiment, an overview of this can be found in Table 2. For the first experiments, flow was the most important factor to consider, so only the big chips designed for flow were used. For the second experiment the emphasis was put on the geometry, so the big chip was compared to the previously used smaller chip. For the third experiment both factors were taken into consideration. To gather as much information as possible, as many chips as could be fabricated in time were used. When flow was applied, the flow was applied to half of the chips per condition, the other half was used as a control.

Table 2: Amount of chips per type that were used per experiment. When flow was used, half of the chips per condition were put on the rocker, the other half was used as control.

	big chip		small chip		
No.	small overlap	big overlap	small overlap	big overlap	flow used
1	4	4	-	-	yes
2	3	2	2	-	no
3	6	4	6	6	yes

The Leiden University Medical Centre (LUMC) provided the human induced Pluripotent Stem Cells (hiPSCs, line LUMCi0054-A). This stem cell line has been defined and registered in the human Pluripotent Stem Cell registry (https://hpscreg.eu/cell-line/LUMCi001-A). The karyotype of the cell line has been analyzed by G-banding, and the cell line shows spontaneous in vitro differentiation to endoderm, mesoderm and ectoderm.
The differentiation was done by the chair Applied Stem-cell Technologies (AST, University of Twente) using previously reported protocols [23]. In short, using a non-integrative Sendai Virus, human kidney epithelial cells (LUMCi0054-A) were reprogrammed to hiPSCs and redirected to endothelial fate by growing the hiPSCs on matrigel and exposing the hiPSCs to medium containing bone morphogenetic protein 4, activin A, CHIR99021 and vascular endothelial growth factor (VEGF) followed by culture in medium supplemented with VEGF and transforming growth factor-β inhibitor (SB431542). Only differentiated ECs were extracted from the heterogeneous culture, by using magnetic CD31-specific Dynabeads (Invitrogen). The expanded ECs were frozen

in 40% EGM-2 (Promocell), 10% dimethyl sulfoxide and 50% fetal calf serum (v/v) to be thawed upon use. Differentiated endothelial cells have previously been extensively characterized using FACS, immunofluorescence and RNA sequencing, and have a distinct phenotype that mostly resembles an embryonic state, but also shows signs of an arterial phenotype [23].

Cells were expandded in a T-75 bottle (Cellcoat, Collagen Type I, 65890, Griener Bio-one, USA) with freshly made medium, consisting of human endothelial serum free medium (EC-FSM, Thermo Fisher Scientific, Massachusetts, USA) supplemented with 40 ng/mL vascular endothelial growth factor (VEGF, Miltenyi Biotec, Bergisch Gladbach, Germany), 20 ng/mL human fibroblast growth factor (hFGF, Miltenyi Biotec, Bergisch Gladbach, Germany) and 1 v/v% platelet-poor serum (Biomedical Technologies, Madrid, Spain) which had been filtered, to prevent cell re-differentiation.
After about 48-72 hours, typically a confluency of 90% was reached. After which the cells were washed with PBS, then the cells were detached, by using trypsine (TrypLE Select (1X), Thermo Fisher Scientific, New York, USA) and incubating for 3 minutes. After detachment, 6 mL of EGM was added to neutralize the trypsine and the cells were centrifuged for 5 minutes at 390 rpm. Subsequently the medium was taken off the pellet and the cells were re-suspended to obtain a concentration of $5 \cdot 10^6$ cells/mL, which for the third experiment was heightened to $8 \cdot 10^6$ cells/mL.
10 µL of endothelial growth medium (EGM-2, SigmaAlderich Chemie GmbH, Steinheim, Germany) was added to the top channel and 10 µL of the cell-solution was added to the bottom channel of the chip. Immediately, the chip was put upside-down, the first experiment without pipette points inside, the second and third experiments the chips were balanced on the pipette tips, and incubated for 60 minutes at 37°C and 5% carbon dioxide (CO_2), to allow for adhesion to the membrane. Once the cells were attached to the membrane, typically after 1-2 hours, medium was refreshed by pipetting 50 µL in the channels and flipping the chips right-side-up again. After 1 day (approximately 24 hours) of cell culture in chip, for the first and third experiment half of the chips were put on the rocker at 24° and 15 and 5 rpm respectively to initiate flow. For all experiments medium was refreshed everyday, for the third experiment twice per day, 4.5 days after seeding fixations were performed. First both channels were flushed with PBS thrice. The cells were fixed with formaldehyde 4%, by leaving the chips at room temperature (RT) in a closed space for 15 minutes. Once cells were fixed, they were flushed with PBS thrice. 2 days after seeding, the cells were stained. First the cells were permeabilized with 0.3% Triton-X and 5% bovine serum albumin (BSA, A7030, Sigma Aldrich, USA) for 30 minutes at RT. After washing with PBS thrice again, the channels were flushed with the primary antibodies (ABs) for EC culture anti-ZO-1 (rabbit polyclonal, 1:100 dilution, 61-7300, Thermo Fisher Scientific, Massachusetts, USA) in 0.5% BSA and monoclonal VE-cadherin (VE-Cadherin antibody F-8, mouse monoclonal IgG, 200 µg/mL, sc-9989, Santa Cruz Biotechnology) at concentrations of 100:0.5:1 µL PBS:antibodody VE-Cadherin:antibody ZO-1. After incubating overnight at RT, the cells were again washed thrice with PBS, subsequently the cells were incubated with secondary antibodies Alexa Fluor 647 donkey anti-rabbit (1:500 dilution, A31573, Thermo Fisher Scientific, Massachusetts, USA) for ZO-1, Alexa Fluor 488 anti-mouse (1:500 dilution, Thermo Fisher Scientific, Massachusetts, USA) for VE-Cadherin and, ActinRed and NucBlue (2 drops per milliliter, Thermo Fisher Scientific, Massachusetts, USA).

3.3 Analysis

After washing the chips thrice with PBS, they were imaged using phase-contrast microscopy (EVOS m5000, Invitrogen, Thermo Fisher Scientific, Massachusetts, USA) and confocal microscopy (FLUOVIEW FV3000, Olympus, confocal laser scanning microscope).
To quantify the monolayer, *ImageJ* was used, first the image was cropped to contain just the channel, after the freehand selection was used to measure the amount of pixels, which contained cells. This was then divided by the total amount of pixels in the image, to obtain a ratio between 0 and 1, where zero is no cells and 1 is a complete monolayer. The first five chips have been calculated thrice and once with confocal, to determine if there is a big intrapersonal deviation and if there is a difference between the EVOS and confocal images. The rest of the chips have been calculated once. The process is also shown in Figure 5
The channel with the nuclei (DAPI channel, excitation wavelength of 461 nm) has also been examined with *ImageJ*, setting a treshold for the nuclei manually, as the fluorescence differed per image, and a binary picture was required for the next step. The treshold was determined based on when the nuclei where inside the treshold and the background outside the treshold. After, the option *Analyze Particles* was selected, which counted the particles. This process is shown in Figure 6.

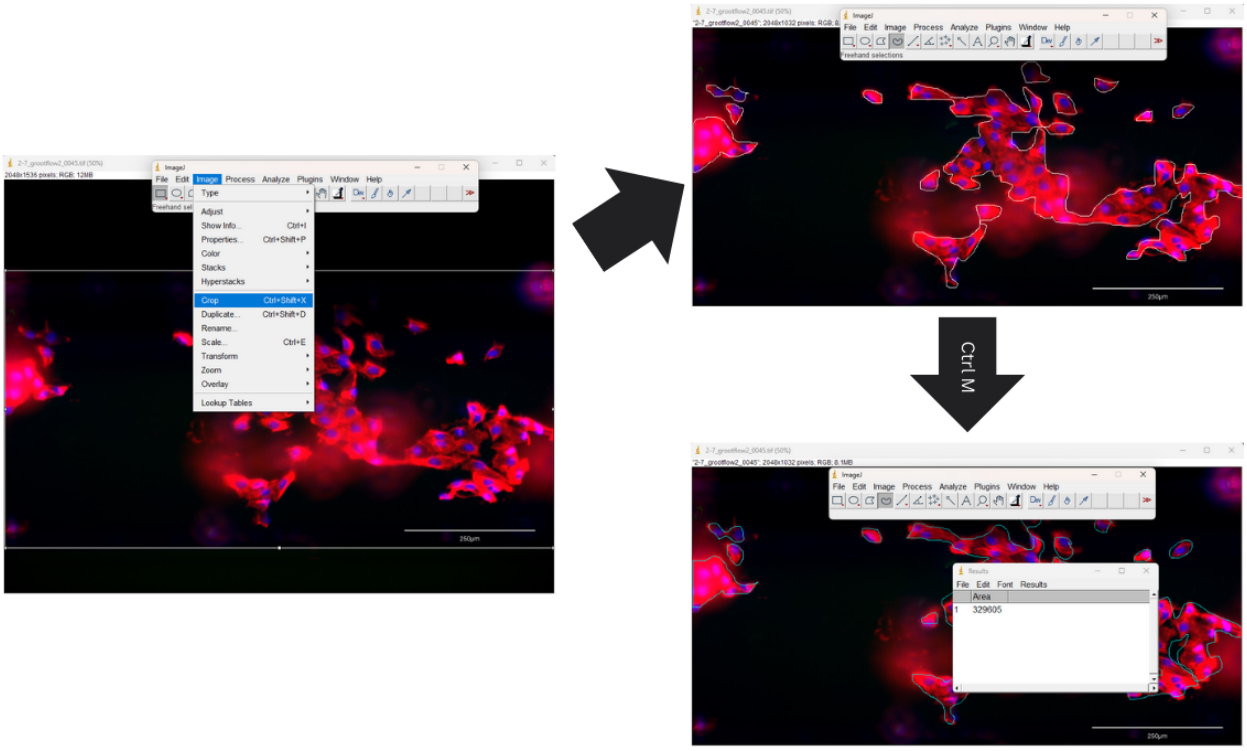

Figure 5: The steps that were taken to recieve an area count for the analysis of the monolayer. Between step 2 and 3 the keys 'Ctrl' and 'M' were pressed to obtain a measurement of the selected area.

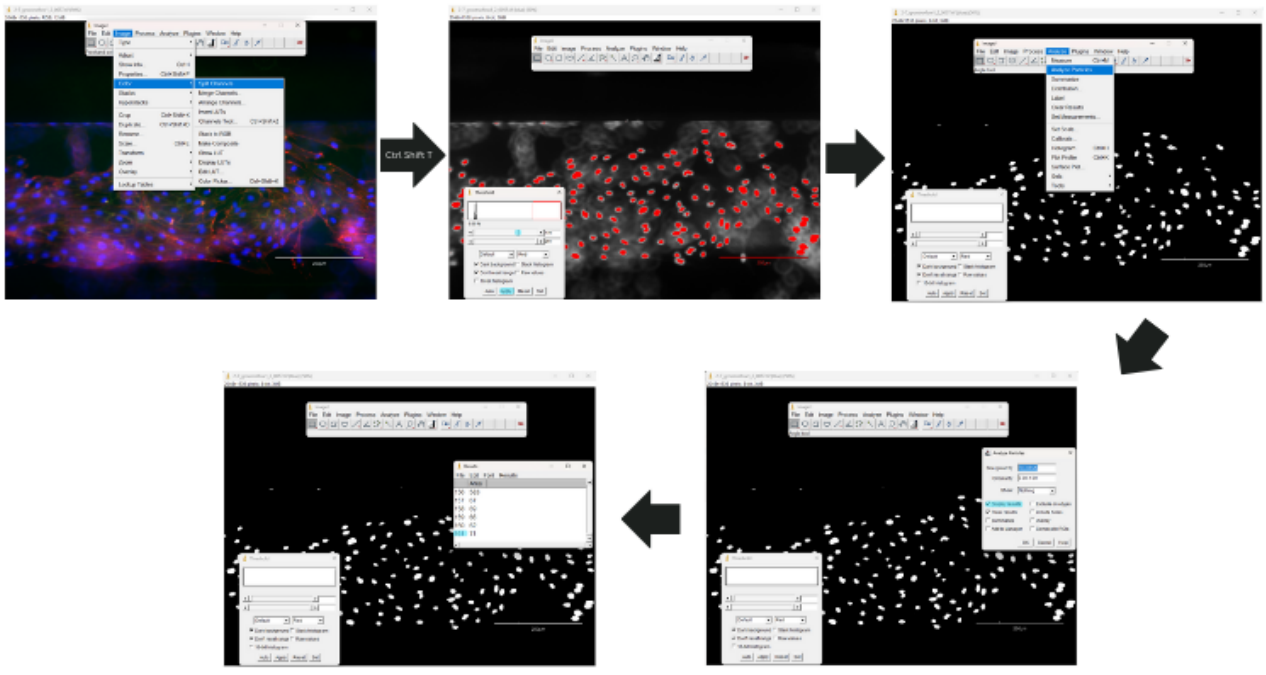

Figure 6: Steps that were taken to get a count of the nuclei. To get to step 2, the keys 'Ctrl' 'Shift' and 'T' were pressed at the same time. During step two, the slide was slid to a point where the nuclei were all red, but not the background.

3.4 Results

Experiment 1: After the first round of experiments, no cells could be observed in the channels. After staining, no nuclei could be observed either. However, what could be observed was some kind of cracking, as shown in Figure 7. For both the big and small overlap, 1 of the 4 chips had this cracking, for the big overlap chip with cracking a flow had been applied (Figure 7a), whereas for the small overlap chip that had cracking, no flow was applied (Figure 7b). The small overlap chip also demonstrates that the cracking did not happen solely in the channels.

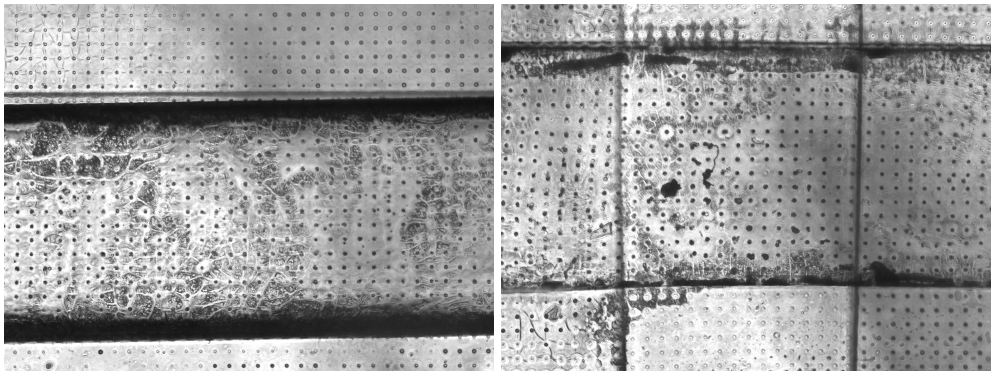

(a) Cracking in the big overlap. (b) Cracking in the small overlap.

Figure 7: Cracking that could be seen in 25% of the chips, it can be observed that the cracking does not happen only in the channels.

Experiment 2: After the second experiment all conditions had 1 chip left without cells. As shown in Table 3, the percentage of chips with cells inside did not differ substantially between the chips. All of the chips that had cells are shown in Figure 8. At the seeding concentration used ($5 \cdot 10^6$), the small chip had a higher cell density, as can be seen in Figure 8d and as shown by the confluence in Table 3.

Table 3: Confluence and cell percentage per chip type.

Type chip	Percentage chips with cells	Confluence
Big chip with big overlap	50% (n=2)	5-10%
Big chip with small overlap	66.7% (n=3)	10%
Small chip with small overlap	50 % (n=2)	80 %

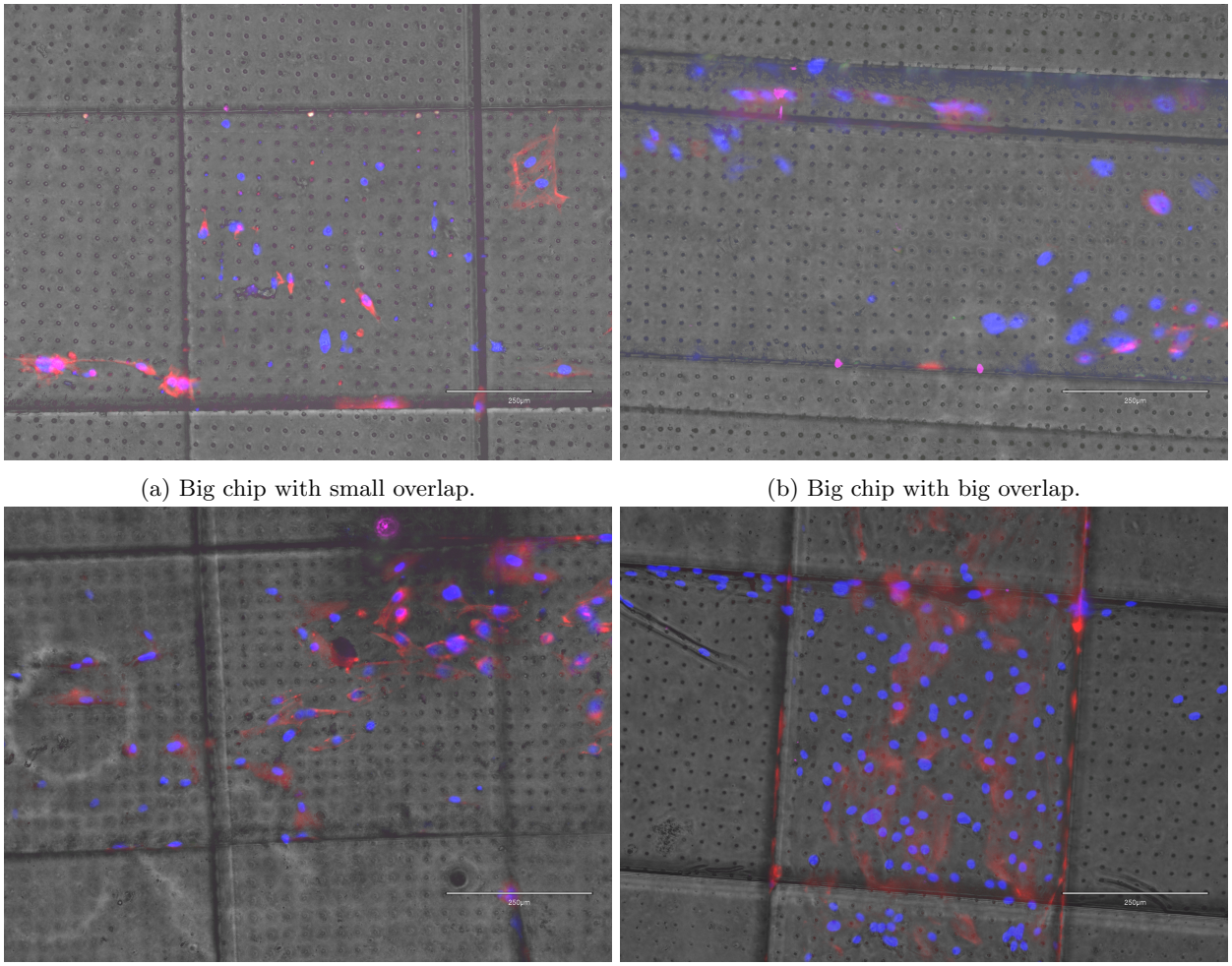

(a) Big chip with small overlap.

(b) Big chip with big overlap.

(c) Big chip with small overlap.

(d) Small chip with small overlap.

Figure 8: Chips with cells inside. Nuclei are colored in blue, actin filaments in red, ZO-1 junctions in purple.

Experiment 3: In Figure 9, the amount of cells inside the chip after a certain amount of days can be seen. Between day 3 (9b) and day 4 (9c) a hole on the bottom can be seen to appear. When imaging with the EVOS, even less cells are present (9d).

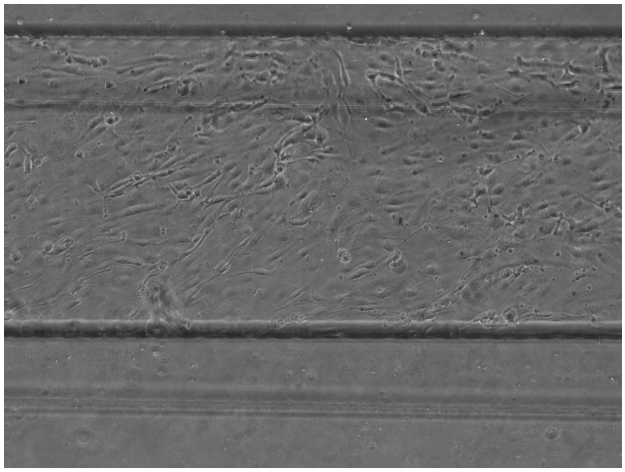

(a) Approximately 1 day after seeding.

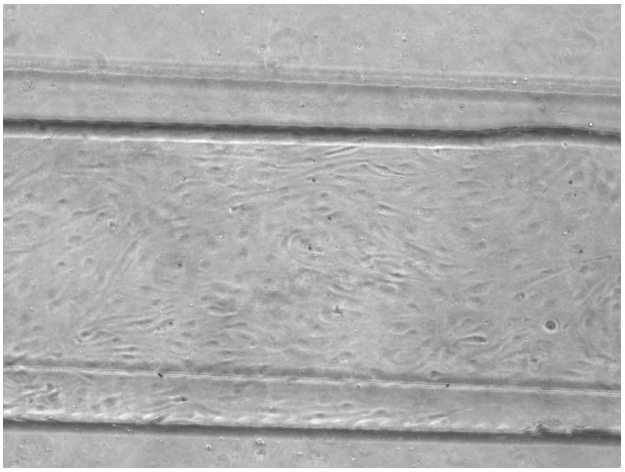

(b) Approximately 3 days after seeding.

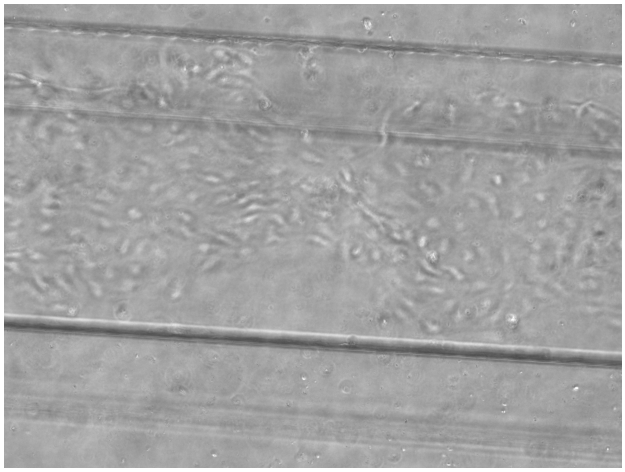

(c) Approximately 4 days after seeding.

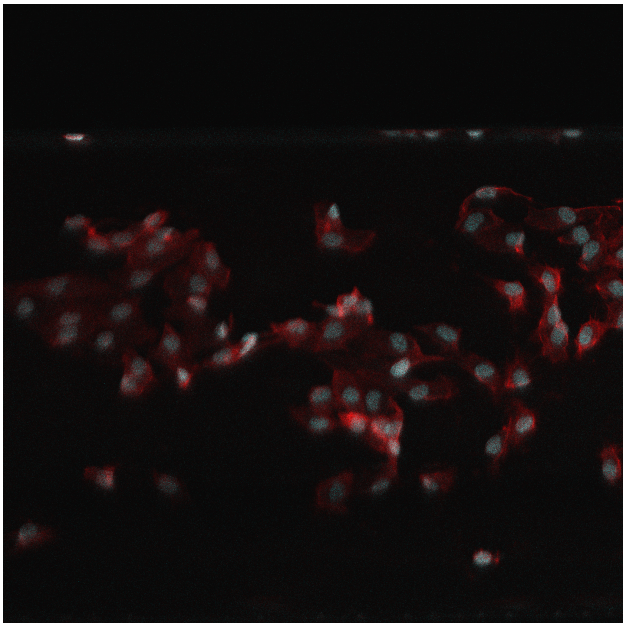

(d) EVOS, fixed 4.5 days after seeding.

Figure 9: Diminishing of cells after 3 days in a big chip with a big overlap.

In some of the chips the washing out of the cells could be seen, due to the cells not forming a complete monolayer in the overlap, but just a few micrometer further into the channel, there would be an almost complete monolayer. An example of this can be seen in Figure 10. This process is most obvious in the chips with the small overlaps.

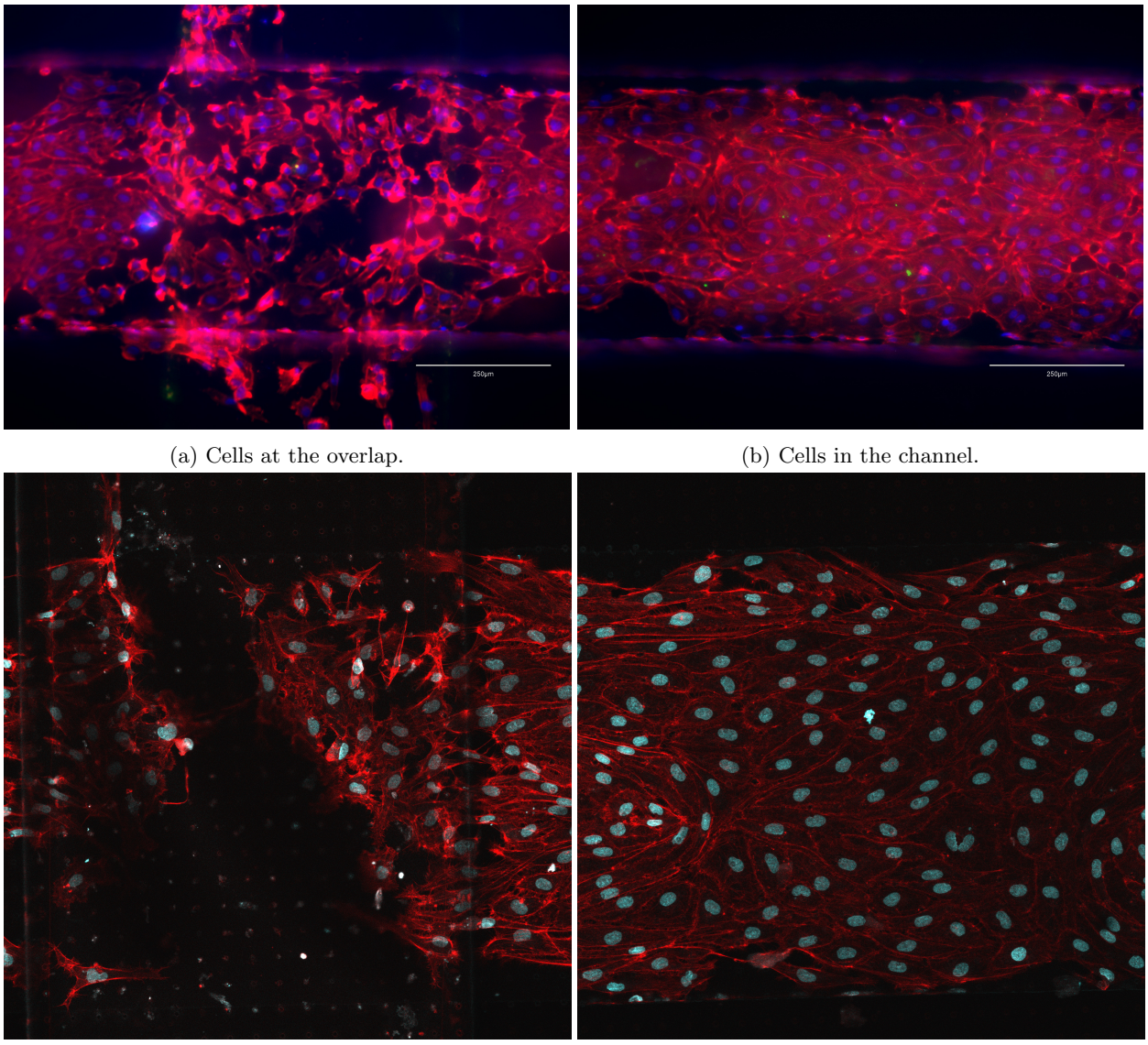

(a) Cells at the overlap.

(b) Cells in the channel.

(c) Cells at the overlap.

(d) Cells in the channel.

Figure 10: A comparison of the monolayer at the overlap and in the channels. (a) and (b) were made with the EVOS, (c) and (d) were made with the confocal.

While using the confocal, it was noticed that not all of the cells were in the same plane of focus. After making a z-stack it could be sliced to reveal where in the channel the cells were located. The result of this is in Figure 11. It can be seen that there is a wave in the monolayer, due to a wave in the membrane. In multiple chips there were also two layers, one on the membrane and one at the bottom of the channel. This can also be seen in Figure 11.

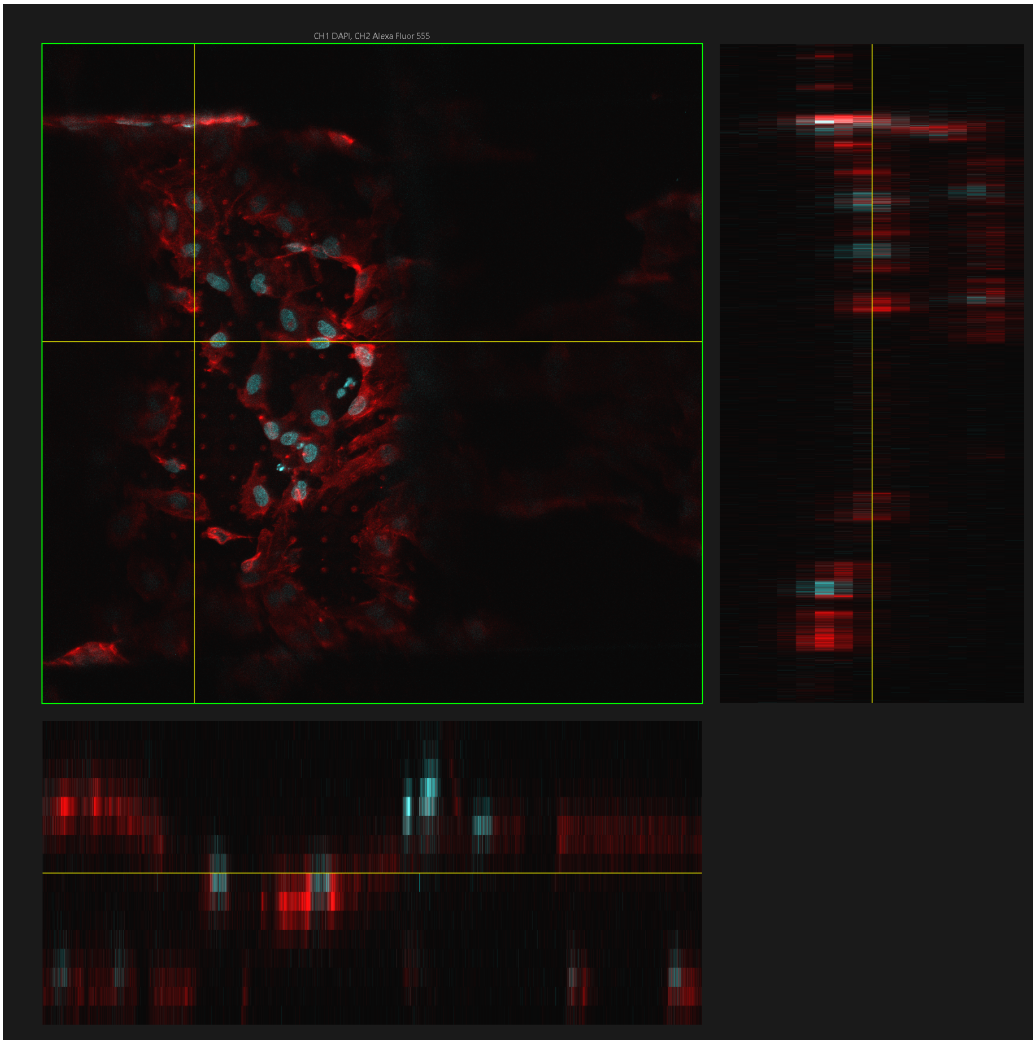

Figure 11: a z-stack picture that has been sliced in the length to reveal the wave in the membrane in x, y, and z directions. The yellow lines are where the z-stack was sliced, the result of this slicing can be seen on the bottom and right.

In Figure 12, a comparison of the confluence of the cell monolayer is made. The empty chips are disregarded, thus the amount of data points differs per condition. It can be seen that there is a high level of variability inside the conditions. The small chips have a higher confluence than the bigger chips. For the big chips, the big overlap with no flow chips have a higher confluence than the chips with flow applied, whereas for the smaller overlap the flow condition has a higher confluence than the no flow condition. Overall the flow condition has a higher confluence than the no flow condition. For the comparison between the big and small overlap, the difference seems to be minimal.

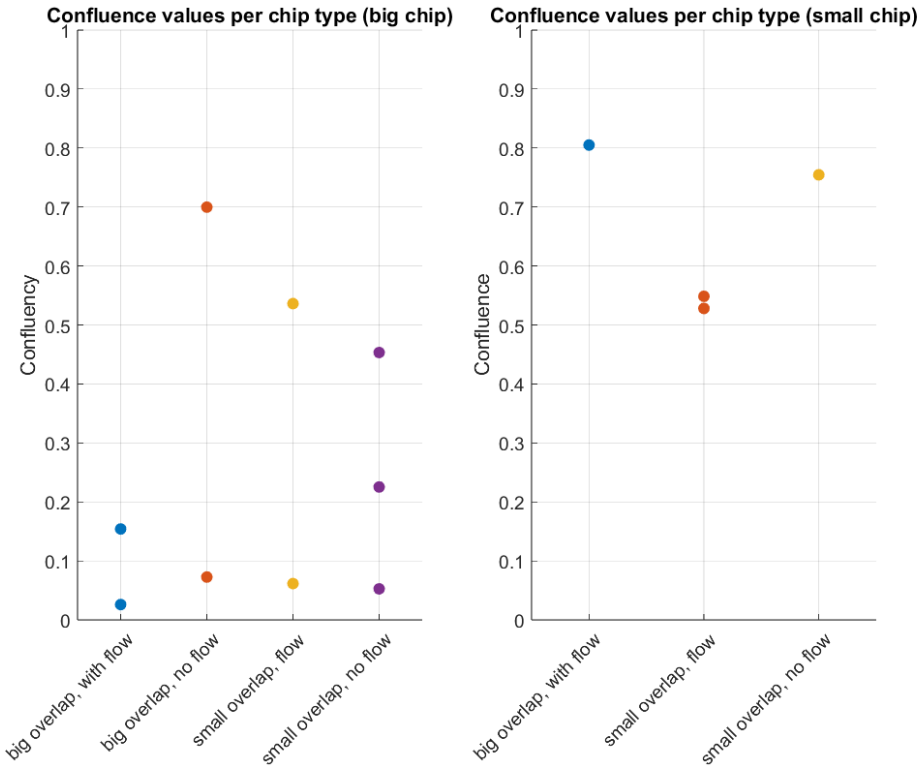

Figure 12: The confluency per chip type, with the big chip on the left and the small chip type on the right.

To ensure the validity and reliability of the data, the confluency has been plotted against the amount of nuclei. If the data is valid and reliable this results in a linear relationship, as can be seen in Figure 13.

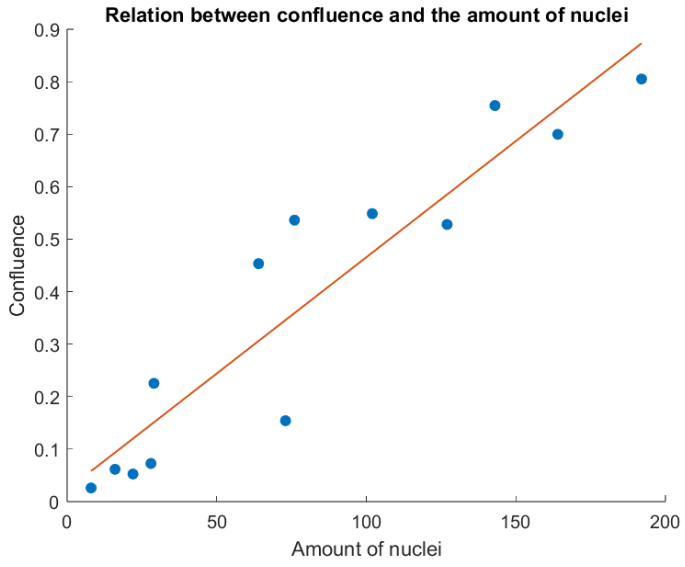

Figure 13: The relation between the amount of nuclei and the confluence. A linear trendline has been drawn in the scatterplot.

4 Discussion

4.1 Chip Design

The original design was based on the rocker being able to provide an angle of 48 degrees, however the rocker provided a 48 degree angle between it's maximum positions, which is only a 24 degree when related to the horizontal axis. Using the 24 degree angle, it was already noticed that the chips needed to be padded with paper to prevent them from toppling over, especially the small ones, thus a higher rocker angle might be more challenging to carry out.
The derivation of the shear stress formulas approached the slope as a linear slope, when in reality it has a parabolic shape, this will result in slightly higher shear stress values on the chips than calculated.
The resistance in the chips seemed to differ between chips. When putting them at an angle and monitoring how quickly the liquid would go from one pipette tip to the other, a difference in time could be seen between chips. This could have been due to how deep pipette points were inserted, as it was possible for the pipette points to close the inlet, as could be seen when trying to pipette in medium, which would not work until the pipette points were pulled out more. However, with a thin chip, sometimes the inlet height was so low that the pipette tips would barely keep upright when inserted. So a correct balance needed to be found, which differed per chip, as not all chips were of equal height.
Chips with a lower height are better for the MB+FUS experiments, as these are imaged with confocal which has a maximum depth the laser can reach, dependent on the objective used. However, as mentioned, lower chips can result in less flow due to the pipette insertion. A way to reduce this problem could be to cut the pipette tips diagonally, allowing one side to be longer for support, while the other is open for the medium to flow through.

4.2 Technical

Experimental
In experiment 1 the chips were put upside down on an empty pipette box. Due to gravity, this caused the cells to leak out. This was solved by balancing the chips on pipette points in experiment 2 and 3, as the hydrostatic pressure in the pipette tips will allow the medium with cells to stay in the channels.
The cracking that could be seen in Figure 7, could have been caused by the collagen coating, as cracking of collagen has been recorded previously [24, 25, 26]. However, it should not pose a problem to the cell culture, as collagen has self-healing effects [26]. Thus it is safe to assume that the reason the cells disappeared is due to the leaking out.
In the second experiment, trypsine was left on too long, which can be assumed to be the reason that about half of the cells died after less than one day after seeding, as the trypsine causes proteins to be digested, leaving it on too long could result in too many proteins to be destroyed, leaving the cell unable to perform it's basic functions, causing it to self-destruct.

Analysis
The intrapersonal deviation for the monolayer quantification resulted in an average standard deviation of 0,00627 when not taking into account the confocal images. When also using the confocal image, the average standard deviation goes up to 0,04024. This is probably due to the confocal images having been made half a week later, which could have let some of the cells disintegrate. Therefore only the EVOS pictures have been used for the analysis. The standard deviation for the EVOS pictures is small enough that the intrapersonal deviation does not make the data less accurate. When letting *ImageJ* determine the amount of cells, some nuclei were overlapping, causing them to be counted as one. This could have resulted in lower cell counts for some of the chips.
In the third experiment, it could be seen that some of the membranes were wavy, as shown in Figure 11. This does not impact the cells or monolayer formation, however the confocal has a very small focus point, which results in the cells not to be in focus. By opening the aperture further, the plane of focus widened, however this resulted in a lower spatial resolution, which was not a problem for the analysis. A probable reason for the membranes to be wavy, was that a defect membrane was applied first and upon inspection, this membrane was taken off and the new one applied, but some of the residue of the defect membrane could have been left, which, when the new membrane was applied, could have caused the new membrane to wave over it.

4.3 Recommandations

After three days, the monolayer started to get holes, as demonstrated in Figure 9, it is therefore recommended to perform bubble studies after 3 days. This could be seen in almost all of the chips, thus pointing at it being a systemic issue, either with the cell line, with the conditions, or with an infection. For further studies the chips should be monitored to see if this phenomenon occurs more often, and if this is the case, conditions should be

varied to find out what exactly is causing it.
A lot of the smaller chips (66,67%) were leaking, which caused the channels to get airbubbles and the cells to die. This could be due to the design of the chip, but it could also be due to a technical mishap, as the PDMS seemed more flexible, which could have been caused by incorrect mixing with the curing agent.
The smaller chips have a bigger cross-section as the width is 500 µm and the height is 375 µm, compared to the bigger chips with the width of 500 µm and a height of 200 µm. The chips were seeded at the same concentration, but due to the bigger cross-section of the smaller chip, the cell density was higher in the smaller chips. In the second experiment week the cell density was even lower and subsequently, the monolayer had a lower confluence. This suggests that the cell density is an important factor in the monolayer formation and maintenance. To find the optimal cell density more research should be done with different cell density's. Due to the smaller chips having a higher cell density, the comparison between the bigger and smaller chips is not accurate when looking at chip design as not all other conditions were the same. The seeding concentration was the same, but not the seeding density.
As can be seen in Figure 12, there is a big spread inside of conditions, not just between conditions. This is a notable occurance, as within a condition all cells were treated the exact same, such as being in the same enclosure, being on and off the rocker at exactly the same times and having their medium refreshed right after each other or at the same time. Cell detachment could be due to either something with the cells and the incubation, which is not likely as all cells came from the same stock and where treated the same, especially within conditions, or due to something with the surface. It is possible that the collagen coating worked better in some of the chips, as all of the chips were first put in the plasma bonding machine in groups and only after all of the chips had been made hydrophilic were coated with collagen. Due to the length of this process it is possible that the chips that were coated last were not as hydrophilic anymore, which could have resulted in the channel not being coated with collagen as well and thus being more hydrophobic when cells were put in. Cells don't attach to hydrophobic surfaces, so this could be a reason that some of the cells detached.
It could also be due to iPSC's being very delicate cells, and small changes, like being dry for some time or getting a tap could result in the cells detaching or dying.
Another option could be that the higher resistance due to some pipette tips, which was discussed earlier, resulted in the cells not getting enough nutrients as they could only access the medium that was already in the channel and not the medium in the reservoir. Or this could have meant that when the chips were put on the rocker, there was considerably less flow than calculated. Depending on for which chips this was the case, it could mean that the chips which did not get as much flow did better or the chips which did get flow did better. However the spread can also be seen in the no flow conditions, as such it is probably not due to the flow.
To determine what was the cause of the spread and whether flow could have a positive effect more research needs to be done. One part of the research should be determining the reason for the high variability even inside of conditions by focusing on one of the conditions used in this research and researching whether the oxygen plasma treatment and collagen coating needs to happen chip per chip, to let it be as quick as possible. It could be researched if the oxygen plasma treatment is equally succesfull in each chip by checking the wettability/hydrophilicity of the channel after the treatment. Another part would be determining if flow could support monolayer formation and maintenance by focusing on one chip and having a higher number of chips, instead of having many different chips with less chips per condition. It can then be seen whether the high variability was due to one of the chips being an outlier.
It should also be noted that the flow used was a bidirectional flow on a rocker, where most sources used unidirectional flow with a flow pump. The rocker was chosen as it makes for a simpler setup which could be used in combination with MB+FUS experiments. However there is ongoing debate if bidirectional flow is beneficial or not [27, 28].

5 Conclusion

The problem to solve, the washing out of the cells at the overlap of the channels, has not been solved, as this was shown to happen still. This happens after three days. In regards to the application of flow, the data has a high level of variability, thus not a clear conclusion can be drawn. A clear difference can be seen between the big and small chips in confluency, suspected to be due to the higher cell density in the smaller chips. It is recommended to apply the knowledge gained to a more focused research.

Acknowledgements

During the preparation of this work, I used ChatGPT to rewrite sentences to sound more professional and academic and less like talking language. I also used it to write a script to put the data points into a graph, specifically Figure 12. After using this tool, I thoroughly reviewed and edited the content as needed, taking full responsibility for the final outcome. I also used Biorender to make the figures 2, 3, and 4a.

References

[1] Persidsky Y, Ramirez S, Haorah J, Kanmogne G. Blood–brain Barrier: Structural Components and Function Under Physiologic and Pathologic Conditions. Journal of neuroimmune pharmacology : the official journal of the Society on NeuroImmune Pharmacology. 2006; DOI: 10.1007/s11481-006-9025-3.

[2] Jena L, McErlean E, McCarthy H. Delivery across the blood-brain barrier: nanomedicine for glioblastoma multiforme. Drug Delivery and Translational Research. 2019; DOI: 10.1007/s13346-019-00679-2.

[3] Delsing L, Herland A, Falk A, Hicks R, Synnergren J, Zetterberg H. Models of the blood-brain barrier using iPSC-derived cells. Molecular and Cellular Neuroscience. 2020;107:103533. DOI: https://doi.org/10.1016/j.mcn.2020.103533.

[4] Yan L, Moriarty RA, Stroka KM. Recent progress and new challenges in modeling of human pluripotent stem cell-derived blood-brain barrier. Theranostics. 2021;11:10148-70. DOI: 10.7150/thno.63195.

[5] Zhao Y, Gan L, Ren L, Lin Y, Ma C, Lin X. Factors influencing the blood-brain barrier permeability. Brain Research. 2022;1788:147937. DOI: https://doi.org/10.1016/j.brainres.2022.147937.

[6] Chakroun RW, Zhang P, Lin R, Schiapparelli P, Quinones-Hinojosa A, Cui H. Nanotherapeutic systems for local treatment of brain tumors. WIREs Nanomedicine and Nanobiotechnology. 2018;10(1):e1479. DOI: https://doi.org/10.1002/wnan.1479.

[7] Song KH, Harvey BK, Borden MA. State-of-the-art of microbubble-assisted blood-brain barrier disruption. Theranostics. 2018;8:4393-408. DOI: 10.7150/thno.26869.

[8] Passeri E, Elkhoury K, Morsink M, Broersen K, Linder M, Tamayol A, et al. Alzheimer's Disease: Treatment Strategies and Their Limitations. International Journal of Molecular Sciences. 2022;23(22). DOI: 10.3390/ijms232213954.

[9] Perkins A, Liu G. Primary brain tumors in adults: Diagnosis and treatment. Am Fam Physician. 2016; DOI: DOI: 10.2174/1389201014666131226114611.

[10] Zakharova M, Van Den Broek MRP, Segerink LI, Segers T. Ultrasound Triggered Bubble-Induced Blood-Brain Barrier Opening: A Monodisperse Microbubble and Organ-On-Chip Study. In: 2023 22nd International Conference on Solid-State Sensors, Actuators and Microsystems (Transducers); 2023.

[11] Mondou P, Mériaux S, Nageotte F, Vappou J, Novell A, Larrat B. State of the art on microbubble cavitation monitoring and feedback control for blood-brain-barrier opening using focused ultrasound. Physics in Medicine Biology. 2023 sep;68(18):18TR03. DOI: 10.1088/1361-6560/ace23e.

[12] Vatine GD, Barrile R, Workman MJ, Sances S, Barriga BK, Rahnama M, et al. Human iPSC-Derived Blood-Brain Barrier Chips Enable Disease Modeling and Personalized Medicine Applications. Cell Stem Cell. 2019;24(6):995-1005.e6. DOI: https://doi.org/10.1016/j.stem.2019.05.011.

[13] Cucullo L, Hossain M, Puvenna V, Marchi N, Janigro D. The role of shear stress in Blood-Brain Barrier endothelial physiology. BMC Neuroscience. 2011; DOI: 10.1186/1471-2202-12-40.

[14] Wang X, Xu B, Xiang M, Yang X, Liu Y, Liu X, et al. Advances on fluid shear stress regulating blood-brain barrier. Microvascular Research. 2020;128:103930. DOI: https://doi.org/10.1016/j.mvr.2019.103930.

[15] Mairey E, Genovesio A, Donnadieu E, Bernard C, Jaubert F, Pinard E, et al. Cerebral microcirculation shear stress levels determine Neisseria meningitidis attachment sites along the blood–brain barrier . Journal of Experimental Medicine. 2006;203(8):1939-50. DOI: 10.1084/jem.20060482.

[16] DeStefano J, Jamieson J, Linville R, Searson P. Benchmarking in vitro tissue-engineered blood–brain barrier models. Fluids and Barriers of the CNS. 2018 12; DOI: 10.1186/s12987-018-0117-2.

[17] Itoh Y, Suzuki N. Control of Brain Capillary Blood Flow. Journal of Cerebral Blood Flow & Metabolism. 2012;32(7):1167-76. DOI: 10.1038/jcbfm.2012.5.

[18] Ivanov KP, Kalinina MK, Levkovich YI. Blood flow velocity in capillaries of brain and muscles and its physiological significance. Microvascular Research. 1981;22(2):143-55. DOI: https://doi.org/10.1016/0026-2862(81)90084-4.

[19] Chen X, Jiang Y, Choi S, Pohmann R, Scheffler K, Kleinfeld D, et al. Assessment of single-vessel cerebral blood velocity by phase contrast fMRI. PLOS Biology. 2021 09;19(9):1-18. DOI: 10.1371/journal.pbio.3000923.

[20] Bruus H. Oxford University

[21] Zakharova M, Carmo M, van der Helm M, Le The H, de Graaf M, Orlova V, et al. Multiplexed Blood-Brain Barrier Organ-on-Chip. Lab on a Chip. 2020 07; DOI: 10.1039/D0LC00399A.

[22] van der Helm M, Odijk M, Frimat JP, van der Meer A, Eijkel J, Van den Berg A, et al. Fabrication and Validation of an Organ-on-chip System with Integrated Electrodes to Directly Quantify Transendothelial Electrical Resistance. Journal of Visualized Experiments. 2017 09; DOI: 10.3791/56334.

[23] Halaidych OV, Freund C, van den Hil F, Salvatori DCF, Riminucci M, Mummery CL, et al. Inflammatory Responses and Barrier Function of Endothelial Cells Derived from Human Induced Pluripotent Stem Cells. Stem Cell Reports. 2018;10(5):1642-56. DOI: https://doi.org/10.1016/j.stemcr.2018.03.012.

[24] Bose S, Li S, Mele E, Silberschmidt VV. Fracture behaviour and toughening mechanisms of dry and wet collagen. Acta Biomaterialia. 2022;142:174-84. DOI: https://doi.org/10.1016/j.actbio.2022.02.001.

[25] Santos S, Emery N, Neu CP, Pierce DM. Propagation of microcracks in collagen networks of cartilage under mechanical loads. Osteoarthritis and Cartilage. 2019;27(9):1392-402. DOI: https://doi.org/10.1016/j.joca.2019.04.017.

[26] Lee SJ, Kim CL. Impact of Tribological Conditions on Collagen Coating Self-Healing. Materials. 2024 03; DOI: 10.3390/ma17061341.

[27] Xanthis I, Souilhol C, Serbanovic-Canic J, Roddie H, Kalli AC, Fragiadaki M, et al. β1 integrin is a sensor of blood flow direction. J Cell Sci. 2019 jun; DOI: https://doi.org/10.1242/jcs.229542.

[28] Kwon EJ, Choi Y, Kim SY, Park S, Yun G, Min SH, et al. Development of Drug Efficacy Testing Platform for Glomerulonephritis.

Appendix

Appendix A

```
L =                 3;                          % in cm
theta =             deg2rad(24);                % rocker angle in degrees
ratio =             2/5;                        % h_channel/w_channel
%velocity =          0.005;                      % in m/s
h =                 0.0002;                     % in m
eta =               1 * 10^-3;                  % in kg/m^3

H               = L * sin(theta);               % in cm
deltaP          = 1000 * 9.81 * H/100           % in Pa
velocity        = ( deltaP * h^2 * (1-0.63*ratio) )/0.00036;
                                                % in m/s
%h               = sqrt( (0.00036*velocity) / (deltaP * (1-0.63*ratio)) )
                                % in m
w               = h / ratio                     % in m
tau             = eta * 4 * velocity / h;       % in Pa
tau2            = tau * 10                      % in dyne/cm^2
velocity2       = velocity * 1000               % in mm/s
```